Biomedical Engineering Letters
https://doi.org/10.1007/s13534-022-00227-x

ORIGINAL ARTICLE

Clinical application of deep learning-based synthetic CT from real MRI to improve dose planning accuracy in Gamma Knife radiosurgery: a proof of concept study

So Hee Park[1] · Dong Min Choi[2] · In-Ho Jung[1] · Kyung Won Chang[1] · Myung Ji Kim[3] · Hyun Ho Jung[1] · Jin Woo Chang[1] · Hwiyoung Kim[2,4] · Won Seok Chang[1]

Received: 24 December 2021 / Revised: 21 March 2022 / Accepted: 21 April 2022

Abstract
Dose planning for Gamma Knife radiosurgery (GKRS) uses the magnetic resonance (MR)-based tissue maximum ratio (TMR) algorithm, which calculates radiation dose without considering heterogeneous radiation attenuation in the tissue. In order to plan the dose considering the radiation attenuation, the Convolution algorithm should be used, and additional radiation exposure for computed tomography (CT) and registration errors between MR and CT are entailed. This study investigated the clinical feasibility of synthetic CT (sCT) from GKRS planning MR using deep learning. The model was trained using frame-based contrast-enhanced T1-weighted MR images and corresponding CT slices from 54 training subjects acquired for GKRS planning. The model was applied prospectively to 60 lesions in 43 patients including benign tumor such as meningioma and pituitary adenoma, metastatic brain tumors, and vascular disease of various location for evaluating the model and its application. We evaluated the sCT and compared between treatment plans made with MR only (TMR 10 plan), MR and real CT (rCT; Convolution with rCT [Conv-rCT] plan), and MR and synthetic CT (Convolution with sCT [Conv-sCT] plan). The mean absolute error (MAE) of 43 sCT was 107.35 ± 16.47 Hounsfield units. The TMR 10 treatment plan differed significantly from plans made by Conv-sCT and Conv-rCT. However, the Conv-sCT and Conv-rCT plans were similar. This study showed the practical applicability of deep learning based on sCT in GKRS. Our results support the possibility of formulating GKRS treatment plans while considering radiation attenuation in the tissue using GKRS planning MR and no radiation exposure.

Keywords Deep learning · Artificial intelligence · Synthetic CT · Gamma Knife radiosurgery · Neuro-oncology

So Hee Park and Dong Min Choi contributed equally to the study and share first authorship.

✉ Hwiyoung Kim
hykim82@yuhs.ac

✉ Won Seok Chang
changws0716@yuhs.ac

[1] Department of Neurosurgery, Brain Research Institute, Yonsei Medical Gamma Knife Center, Yonsei University College of Medicine, 50 Yonsei-ro, Seodaemun-gu, Seoul 03722, Republic of Korea

[2] Center of Clinical Imaging Data Science, Department of Radiology, Yonsei University College of Medicine, 50 Yonsei-ro, Seodaemun-gu, Seoul 03722, Republic of Korea

[3] Department of Neurosurgery, Korea University Medical Center, Korea University College of Medicine, Ansan Hospital, Ansan-si, Republic of Korea

[4] Department of Biomedical System Informatics, Yonsei University College of Medicine, Seoul, Republic of Korea

1 Introduction

Gamma Knife radiosurgery (GKRS) is a single-treatment irradiation session of a cranial lesion using multiple highly-focused gamma-ray beams produced by ^{60}Co sources. GKRS is being used as a treatment modality for various lesions such as benign and malignant brain tumors, vascular diseases, functional diseases, and some of ocular diseases. As it is a high-energy treatment for the brain, accurate irradiation is important. Early GKRS planning was performed with a non-imaging-based stereotactic planning system called KULA using with X-ray, angiography, and computed tomography (CT) [1]. Since it was designed in the pre-computerized imaging era, it was more focused on geometric accuracy and had only limited capacity for dosimetry. This was followed by the Leksell GammaPlan® software, with advanced graphic features and a sophisticated multi-parameter system

Published online: 13 June 2022

[1]. The GammaPlan®, still in use today, calculates the dose based on the tissue maximum ratio (TMR) algorithm that considers the head geometry only.

Once magnetic resonance (MR) imaging was developed and used for clinical applications, with the advantages of soft-tissue contrast and target delineation, it has also been applied to GKRS planning. In addition to the above advantages, MR can image the geometry of the head; therefore, for decades, MR-only workflow was used for GKRS planning. However, the TMR algorithm assumes the patients head is of even water-equivalent density and does not consider the radiation attenuation in the bone. For more precise treatment, the need to consider the patient tissue heterogeneity during planning has emerged. Hence, the Convolution algorithm was developed several years ago [2]. The treatment plan with Convolution algorithm has a 6–15% difference in the maximum dose compared to the plan with TMR algorithm [3, 4]. However, CT is required to use it, and due to the additional radiation exposure, time, costs, patients inconvenience, and the CT/MR registration error of up to 2 mm, the Convolution algorithm is not widely used [5].

Since CT and MR have their respective advantages, several studies have reported skull synthetic CT (sCT) from MR [6, 7]. Recent studies have applied deep learning to sCT from MR, showing excellent results in terms of time and accuracy [6–10]. Studies applying sCT made with deep learning to clinical practice for brain have recently been conducted, but few have used it for GKRS [11–14]. In this study, we investigated the applicability of sCT made with deep learning in dose planning for GKRS, which requires high energy with submillimeter accuracy.

2 Materials and methods

2.1 CT/MR imaging protocol for Gamma Knife radiosurgery

MR images for GKRS planning included gadolinium contrast contrast-enhanced T1-weighted images and T2-weighted images. MR images were acquired with a 1.5 T Philips Achieva dStream (Philips Medical Systems, Best, Netherlands). Contrast-enhanced T1-weighted images were captured with a slice thickness of 1.5 mm from the foramen magnum level to the vertex using a T1-weighted 3D gradient recalled echo sequence with contrast agent (echo time, 4.6 ms; repetition time, 25 ms; flip angle, 30º; voxel size, $1 \times 1 \times 1$ mm^3). The images required for each disease were additionally acquired. CT images were acquired as needed for planning, such as when MR distortion correction was required or when implants generated MR artifacts. CT images were acquired on GE LightSpeed VCT (GE Healthcare Technologies, Waukesha, WI) with a tube voltage of 100 kVP and slice thickness of 1 mm.

2.2 Generation of a deep learning model for sCT

The model was trained using all MR image slices with the corresponding CT slices from MR/CT pairs of the 54 training group subjects, acquired for GKRS planning in our institution. The imaging data was retrospectively reviewed. MR images for deep learning were contrast-enhanced T1-weighted images. Generative Adversarial Networks (GAN)-based model was used for sCT generation.

2.2.1 Image registration

Although the same patients were imaged, the CT and MR images were not aligned because the patient moved or due to modality differences. The image registration process for fitting the CT to MR images was performed using SimpleITK [15–17]. At the first rough registration stage, the centers of the two images were aligned. The center of the MR image was set as the center of rotation through Euler registration. A B-Spline transformation based on Mattes Mutual Information was then applied for the fine registration [18–20]. A gradient descent optimizer with a learning rate of 1.0 was used to find the optimal terminal condition for 100 iterations.

2.2.2 Image preprocessing

After the registration process, the CT and MR images were resampled at $1 \times 1 \times 1$ mm isotropic resolution. The MR images underwent *Z*-score normalization using the mean and standard deviation obtained from the training dataset to stabilize the training process. The Hounsfield unit (HU) values of the CT images were normalized to values between 0 and 1 using min–max scaling, with minimum and maximum values of –1024 HU and 1800 HU, respectively considering the HU of the skull. The CT and MR images were resized to 512×512 pixel.

2.2.3 sCT generation

Pix2Pix is a deep neural network that shows distinguished performance in paired image-to-image translation [21]. All settings followed the original experiments of Pix2Pix except for data augmentation [21] (Fig. 1). Random rotation (± 20 degrees), random scaling ($\times 0.9$–1.1), random translation (± 0.1 pixels), and random horizontal flip were applied to prevent mode collapse and overfitting. The final model received preprocessed MR images as input and generated its corresponding sCT images. The network was implemented using Pytorch 1.4. Adam optimizer with a learning rate of 0.0002 and a batch size of ten was used for optimization. A

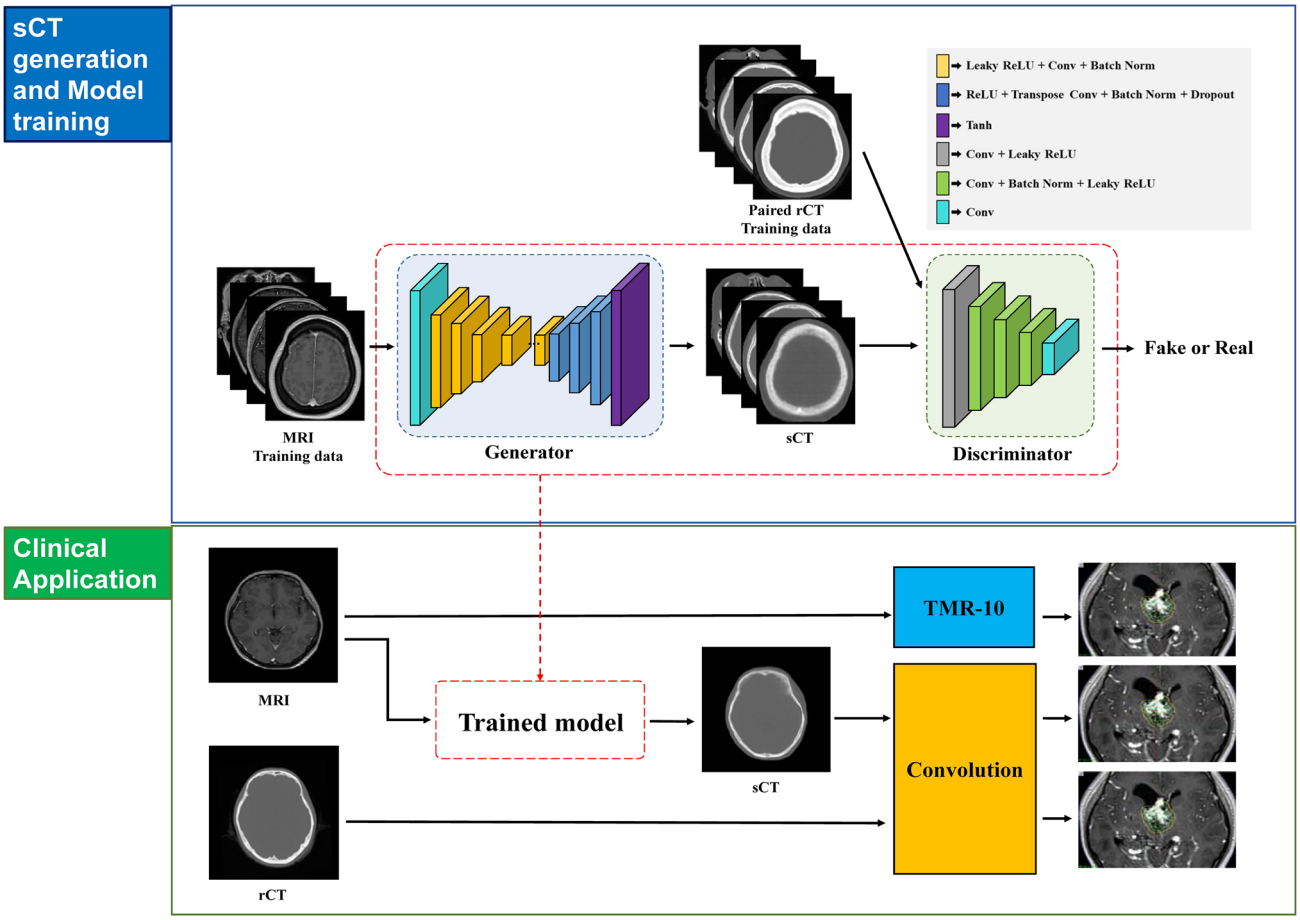

Fig. 1 A schematic illustration of the study. sCT, synthetic computed tomography; ReLU, Rectified linear unit; Conv, Convolution; Norm, normalization

single NVIDIA GeForce GTX 1080 Ti GPU was used for 100 epochs. The memory size of GPU was sufficient since 2D slices were used as an input.

2.2.4 sCT evaluation

The accuracy of the sCT images was measured by voxel-wise mean absolute error (MAE) and structural similarity index measure (SSIM) against the real CT images. The MAE and SSIM could be calculated as follows:

$$\mathrm{MAE} = \frac{1}{n}\sum_{i=1}^{n} |\mathrm{rCT}(i) - \mathrm{sCT}(i)|,$$

and

$$\mathrm{SSIM} = \frac{\left(2\mu_{\mathrm{rCT}}\mu_{\mathrm{sCT}} + c_1\right)\left(2\sigma_{\mathrm{rCTsCT}} + c_2\right)}{\left(\mu_{\mathrm{rCT}}^2 + \mu_{\mathrm{sCT}}^2 + c_1\right)\left(\sigma_{\mathrm{rCT}}^2 + \sigma_{\mathrm{sCT}}^2 + c_2\right)},$$

where n is the total number of voxels, μ_I and σ_I are the mean and standard deviation of image I, and the constants were $c_1 = \{0.01 \times [1{,}800 - (-1024)]\}^2$ and $c_2 = \{0.03 \times [1{,}800 - (-1024)]\}^2$. After confirming the quality of the generated CT images using the above evaluation metrics, the GKRS planning was performed.

2.3 Applying the learning model for preparing the GKRS treatment plan

The study was conducted on patients scheduled to be treated by GKRS who had to undergo MR and CT imaging for planning. Treatment indications included benign tumors such as meningioma (MNG), vestibular schwannoma (VS), and pituitary adenoma (PA), cerebrovascular malformations such as arteriovenous malformation (AVM), and metastatic brain tumors larger than 1 cm^3. The Institutional Review Board of our hospital approved the study before starting it. Written informed consent was obtained from all participants.

2.3.1 Establishment of the GKRS treatment plan

The GKRS plan was created by the GammaPlan® software program (Version 10.1, Elekta AB, Stockholm, Sweden). Importing the image data, skull measurement, and contouring of the target to be treated were performed in the usual way. The GKRS shot plan was calculated and optimized based on the TMR 10 algorithm (a TMR algorithm embedded in GammaPlan®, Version 10.1), and the plan for each lesion was established and adjusted manually by a single surgeon (WSC) with 15 years of experience in GKRS planning. No limit was set for the number of shots or the allowed collimator combination. All targets were prescribed to the 50% isodose line.

2.3.2 Dosimetric analysis

The treatment plan was recalculated with a Convolution algorithm using real CT (rCT) and sCT images (Fig. 1). No adjustment was implemented. Treatment plans were evaluated prospectively for each lesion. The three treatment plans (TMR 10 plan; Convolution with rCT [Conv-rCT] plan; Convolution with sCT [Conv-sCT] plan) were compared for the following evaluation elements of the GKRS treatment plan: coverage (proportion of the target volume covered by the prescription isodose), Paddick conformity index (PCI; how adequately the target was covered by treatment), gradient index (GI; the ratio of the volume enclosed by half of the prescription isodose), and beam-on time (BOT).

2.4 Statistical analysis

Statistical analysis was performed with JMP, Version 9.4 (SAS Inc., Cary, NC, USA). The three treatment plans for each patient were compared using a linear mixed model, and post-hoc analysis was performed with Bonferroni's method. Differences with a p-value smaller than 0.05 were considered statistically significant.

3 Results

The study was performed from August to December 2020 on 60 lesions of 43 patients. These consisted of eight patients with MNG (13.3%), seven with AVM (11.7%), six with PA (10.0%), two with VS (3.4%), and 37 with metastatic brain tumors (61.7%). MNG was variously located, including three lesions of the frontal area. AVM was primarily located in the temporal lobe. Metastatic brain tumors were distributed in the cerebellum, brain stem, and cerebrum, including ten lesions in the parietal lobe and nine in the frontal lobe. The average distance from the vertex to the center of the lesion was 82.1 ± 31.9 mm, and the average target volume was 4.04 ± 3.99 cm^3. Twelve lesions were treated by three fractions, and the rest were treated by a single fraction. Details on the patients and lesions are shown in Table 1.

Table 1 Characteristics and treatment plan parameters for the 60 lesions

Characteristics	Value (n)	Volume (cm^3)	Location (n)		Fractionation		Prescription dose (Gy)
Patients	43 (F 27, M 16)						
Lesions	60	4.04 ± 3.99					
Meningioma	8	2.24 ± 1.52	Frontal	3	Three fractions	3	6.7 ± 0.0
			Ant. Skull base	2	Single fraction	5	14.2 ± 0.4 (14.0–15.0)
			Petrous	1			
			Tocular	1			
			Tentorium	1			
Vestibular schwannoma	2	2.11 ± 1.29	–		Three fractions	2	6.6 ± 0.2 (6.4–6.7)
					Single fraction	0	-
Pituitary adenoma	6	4.45 ± 4.58	–		Three fractions	3	8.4 ± 1.0 (7.5–9.5)
					Single fraction	3	25.0 ± 0.0
Arteriovenous malformation	7	7.46 ± 6.64	Temporal	4	Three fractions	0	-
			Parietal	1	Single fraction	7	16.9 ± 1.1 (16.0–18.0)
			Thalamus	1			
			Brain stem	1			
Metastatic brain tumor (≥ 1 cm.^{3})	37	3.82 ± 3.47	Frontal	9	Three fractions	4	8.7 ± 0.5 (8.0–9.0)
			Parietal	10	Single fraction	33	20.4 ± 1.1 (18.0–22.0)
			Occipital	6			
			Temporal	4			
			Cerebellum	5			
			Brain stem	3			

3.1 Evaluation of the sCT images

sCT images were successfully generated for all patients. It took an average of 26.28 s to generate a CT image from an MR image, including the entire preprocessing operation. An example of sCT is presented in Fig. 2. Quantitatively, for the whole head region, the proposed method achieved an average MAE and SSIM of 107.35 ± 16.47 HU and 0.57 ± 0.06, respectively.

3.2 Dosimetric evaluation

The three treatment plans differed significantly in the coverage, PCI, GI, and BOT ($p < 0.001$ for all). Post-hoc analysis found differences between the TMR 10 and Conv-sCT plans in all four parameters (coverage, PCI, GI, and BOT; $p < 0.001$ for all), and between the TMR 10 and Conv-rCT plans (coverage, $p = 0.023$; $p < 0.001$ for PCI, GI, and BOT). However, no difference was found between the Conv-sCT and Conv-rCT plans ($p > 0.999$ for coverage, PCI, and GI; BOT, $p = 0.742$; Figs. 3, 4, Table 2).

4 Discussion

CT imaging has historically been used as the primary source of imaging data for planning external radiation therapy. The CT images provide an accurate representation of the patient geometry and have the advantage that the CT values can be directly translated to electron densities for radiation dose calculation [6]. For this reason, radiation therapy is based on CT. However, since GKRS is a procedure that deliver higher energy and geometrical accuracy is more important than attenuation, GKRS planning was established based on MR without considering tissue heterogeneity until the 2000s. These planning are not problematic in most cases, but these might result in the radiation reaching the incorrect location with an incorrectly calculated dose and, consequently, delivering insufficient treatment or causing normal tissue toxicity.

Recently, in order to treat more precisely, the Convolution algorithm that considers the electron map was introduced. Since MR cannot provide the electron density information needed for accurate dose calculation, a CT scan is required for its application. However, additional radiation exposure for CT is bound to be risky to the patients. Besides, clinical flow complexities and CT/MR registration errors further complicate the situation.

Efforts have been made to extract CT data from MR images, including atlas-based, voxel-based, and hybrid methods [22–24]. In the past decade after the advent of artificial intelligence (AI), researchers started applying AI to this field as well. Due to the rigidity of the skull and relatively little movement of surrounding structures, the registration and learning of brain MR/CT pairs has advantages over other organs, and many researchers have attempted to apply AI to skull CT. Han first reported the synthesis of skull CT images by applying deep learning to MR images in 2017 [6]. CT images were synthesized from T1-weighted MR images using the convolutional neural network (CNN) method, and the quality of the CT images was better than the conventional synthesis method with an MAE of 84.8 HU. Afterwards, studies using GAN, which has strength in image synthesis compared to other generative models were conducted [25]. Nie et al. and Emami et al. showed promising results with an MAE of 92–95 HU in the skull by applying a GAN-based method [26, 27]. Other studies using various

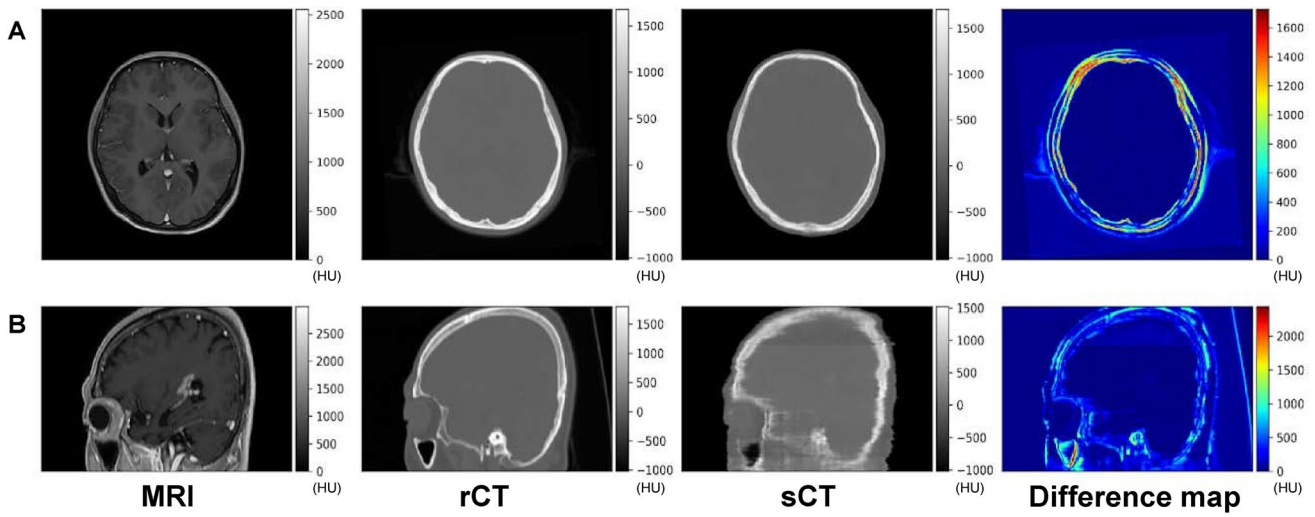

Fig. 2 An example of an axial (**a**) and sagittal (**b**) slice of a magnetic resonance imaging (MRI), real computed tomography (rCT), synthetic CT (sCT), and the difference map between rCT and sCT in a metastatic brain tumor patient

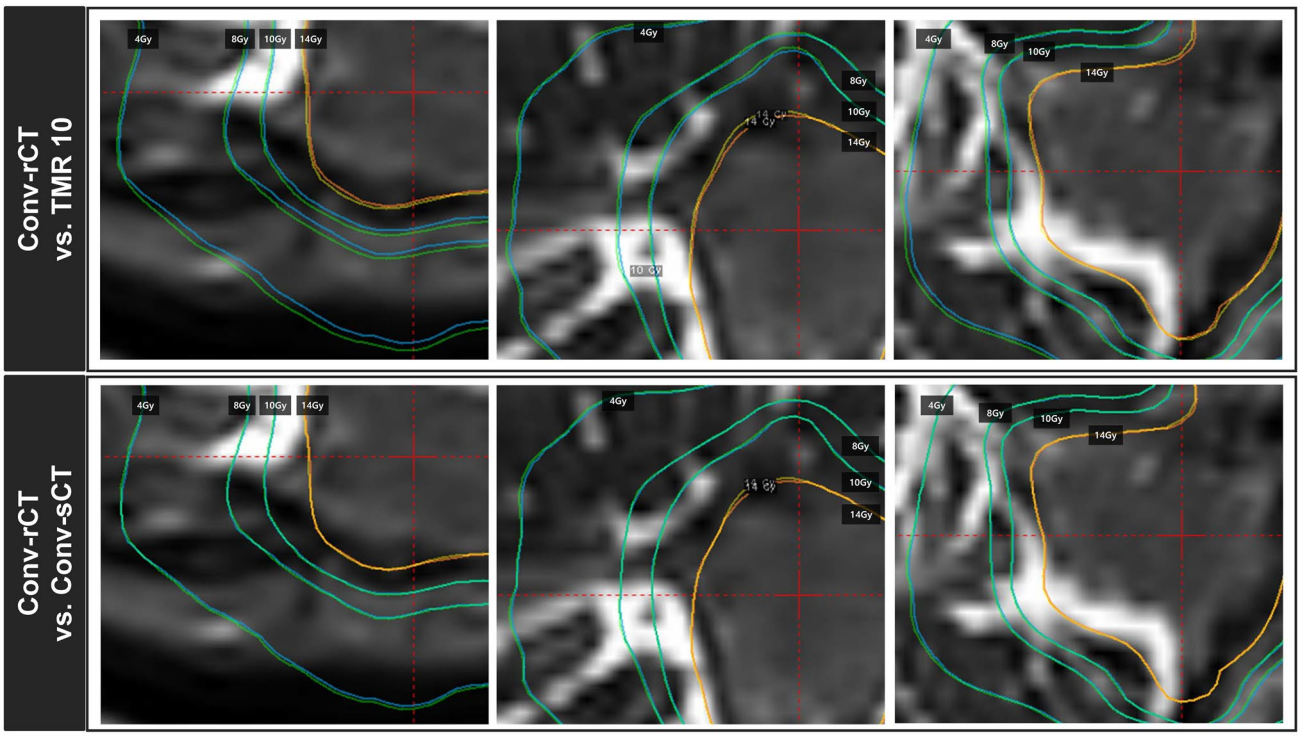

Fig. 3 Comparison between the Convolution with real CT (Conv-rCT) and TMR 10 plans, and between the Conv-rCT and Convolution with synthetic CT (Conv-sCT) plans in a torcular meningioma patient. Conv-rCT plan (orange/blue line) was overlaid with TMR 10 plan (yellow/green line at upper row) or Conv-sCT plan (yellow/green line at lower row)

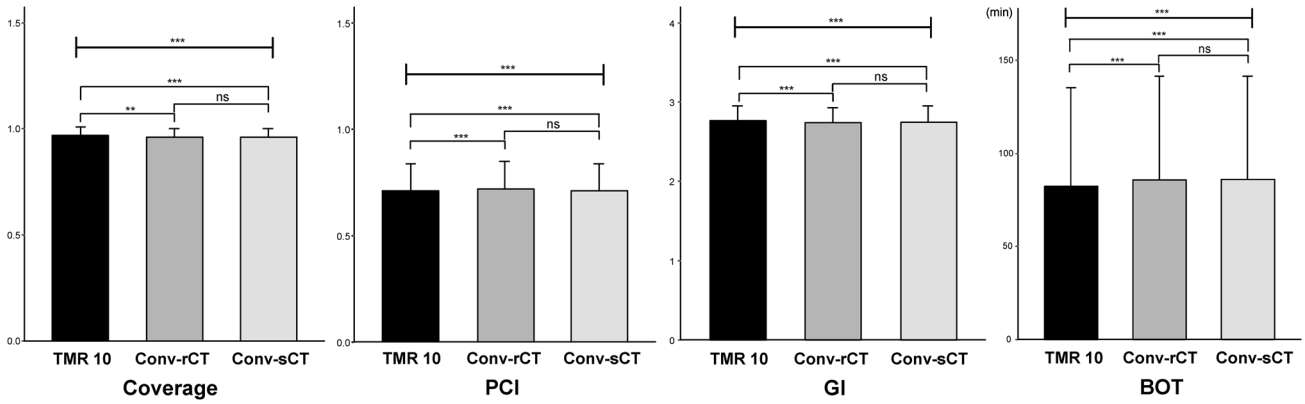

Fig. 4 Comparison between the TMR 10, Convolution with real CT (Conv-rCT), and Convolution with synthetic CT (Conv-sCT) plans. $^{**}p < 0.05$, *** $p < 0.001$. TMR, Tissue maximum ratio; rCT, real computed tomography; sCT, synthetic computed tomography; Conv, Convolution; PCI, Paddick Conformity Index; GI, Gradient Index; BOT, Beam-on time; ns, non-significant

other deep learning methods such as dense cycle GAN or U-net also reported good performance results [7, 8]. The MR sequences used for CT synthesis were various depending on the studies; T1-weighted images with or without contrast, or T2-weighted images. In addition, Dixon, ultrashort echo time (UTE) images, and other sequences that represented bones better are used for better sCT results [6, 9, 10, 28]. As a result, sophisticated sCT images with an MAE of less than 50 HU have been produced currently.

As it is important to make high-performance synthetic CT, its clinical application is also important. GKRS, one of the representative modality of treating cranial lesions, is often performed frame-based for higher accuracy, and for planning MR, 1.5 T MR is preferred with less image

Table 2 Coverage, Paddick Conformity Index, Gradient Index and Beam-on time of the TMR 10, Convolution with real CT (Conv-rCT), and Convolution with synthetic CT (Conv-sCT) plans

	Mean ± SD				*p*-value		
	TMR 10	Conv-rCT	Conv-sCT	Overall	TMR10 vs. Conv-rCT	TMR10 vs. Conv-sCT	Conv-rCT vs. Conv-sCT
Coverage	0.97 ± 0.04	0.96 ± 0.04	0.96 ± 0.04	< 0.001	0.023	< 0.001	> 0.999
Paddick Conformity Index	0.71 ± 0.13	0.72 ± 0.13	0.71 ± 0.13	< 0.001	< 0.001	< 0.001	> 0.999
Gradient Index	2.77 ± 0.18	2.74 ± 0.19	2.75 ± 0.20	< 0.001	< 0.001	< 0.001	> 0.999
Beam-on time	82.45 ± 52.85	85.86 ± 55.62	86.04 ± 55.48	< 0.001	< 0.001	< 0.001	0.742

SD, Standard deviation; TMR, Tissue maximum ratio; rCT, real computed tomography; sCT, synthetic computed tomography; Conv, Convolution

distortion than 3 T MR. Although 3 T MR has better image contrast between tissues and has been widely used in previous studies for more sophisticated images, our study used 1.5 T GKRS planning MR images with a metal frame implemented, which are actually used for GKRS. Since metals form artifacts around in MR, it may cause difficulties in the image learning process and may result in poor sCT results. For this reason, our learning model seems to produce suboptimal results compared to other studies, but it is meaningful in that it was applied to the clinical practice without additional MR implementation and that even sCT with limited performance was sufficient for GKRS planning, showing indistinguishable GKRS plan results from the results with rCT.

So far, the clinical application of sCT made from MR has mainly been in the field of radiation therapy. Dinkla et al. retrospectively studied applying the CNN-based model using T2-weighted MR images to radiation therapy in head and neck cancer patients, and reported MAE of 75 ± 9 HU and less than 1% of mean dose difference in the high dose region of over 90% of the prescribed dose [11]. Lerner et al. synthesized CT using a commercial program with Dixon MR images for 20 brain tumor patients and reported MAE of 62.2 ± 4.1 HU and less than 0.2% of dose differences in parameters evaluated for the targets and organs at risk following volumetric modulation arc therapy (VMAT) plan study [29]. These studies have shown the potential of sCT as an alternative to rCT for radiation therapy.

GKRS is the procedure that deliver a higher dose than radiation therapy, and small differences in sCT can lead to larger dose difference. However, we found no difference in the coverage, PCI, GI, and BOT between the Convolution-based treatment plans formulated with sCT or rCT images. These results support the feasibility of replacing the rCT with sCT for GKRS planning. There was a difference between the Convolution algorithm CT- and TMR 10-based treatment plans. This result was consistent with previous studies showing that Convolution-based and TMR 10-based treatment plans differed by 6–15% of the standard error of maximum dose [3, 4]. This means that when the skull attenuation is considered, there may be a difference in the therapeutic dose for the target compared to when not considered.

Although the Convolution algorithm was developed several years ago for more accurate treatment, it has not been widely used to date, mainly due to the additional CT scan and CT/MR registration error. By showing that planning with sCT in GKRS was similar to that with rCT, our study showed that the planning considering tissue heterogeneity is possible using sCT made by deep learning with only MR. This has lowered the barrier into planning that calculate radiation attenuation in tissue by resolving the difficulty and complexity associated with the additional implementation of CT. By applying this method, it is expected that more accurate dose calculation and treatment considering radiation attenuation in GKRS will be possible without additional inconvenience in the future.

This study has several limitations. First, there is a limit to the generality of the deep learning model. MR images vary significantly across scanner types and a model trained on data from one scanner could not be directly applicable to data from a different scanner. Second, the quality of our sCT is not state-of-the-art. Therefore, additional techniques to improve inter-slice consistency are required for better bone performance [30]. Third, the Convolution algorithm itself may have limitation. Although the algorithm is designed to reflect the electron density, there may be differences from the actual dose.

Author contributions HK and WSC designed the study. HK and DMC created the model. WSC established the treatment plan. SHP, IJ and KWC converted the treatment plan and collected the data. DMC and HK analyzed and interpreted the CT data. SHP, HHJ, JWC and WSC analyzed and interpreted the GKRS data. SHP and DMC drafted the work, and all author reviewed the manuscript.

Funding This research was supported by a grant of the Korea Health Technology R&D Project through the Korea Health Industry Development Institute (KHIDI), funded by the Ministry of Health & Welfare, Republic of Korea (grant number: HI21C1161), the Korea Medical Device Development Fund (Project Number: 202011D25), and Severance Hospital Research Fund for Clinical Excellence (SHRC). The sponsor of the study had no role in study design, data collection, data analysis, data interpretation, or writing of the report. The corresponding authors had full access to all the data in the study and had final responsibility for the decision to submit for publication.

Data availability statement The data generated during the current study are available from the corresponding author on request.

Declarations

Conflict of interest The authors have declared that no conflict of interest exists.

Ethic approval This study was performed in line with the principles of the Declaration of Helsinki. Approval was granted by Institutional Review Board of Severance Hospital (No. 4–2020-0325).

Consent to participate Informed consent was obtained from all individual participants included in the study.

References

1. Ganz JC. The history of the gamma knife. Elsevier; 2014
2. Xu AY, Bhatnagar J, Bednarz G, et al. Gamma Knife radiosurgery with CT image-based dose calculation. J Appl Clin Med Phys. 2015;16(6):119–29. https://doi.org/10.1120/jacmp.v16i6.5530.
3. Fallows P, Wright G, Harrold N, Bownes P. A comparison of the convolution and TMR10 treatment planning algorithms for Gamma Knife((R)) radiosurgery. J Radiosurg SBRT. 2018;5(2):157–67.
4. Osmancikova P, Novotny J Jr, Solc J, Pipek J. Comparison of the convolution algorithm with TMR10 for Leksell gamma knife and dosimetric verification with radiochromic gel dosimeter. J Appl Clin Med Phys. 2018;19(1):138–44. https://doi.org/10.1002/acm2.12238.
5. Ulin K, Urie MM, Cherlow JM. Results of a multi-institutional benchmark test for cranial CT/MR image registration. Int J Radiat Oncol Biol Phys. 2010;77(5):1584–9. https://doi.org/10.1016/j.ijrobp.2009.10.017.
6. Han X. MR-based synthetic CT generation using a deep convolutional neural network method. Med Phys. 2017;44(4):1408–19. https://doi.org/10.1002/mp.12155.
7. Lei Y, Harms J, Wang T, et al. MRI-only based synthetic CT generation using dense cycle consistent generative adversarial networks. Med Phys. 2019;46(8):3565–81. https://doi.org/10.1002/mp.13617.
8. Gupta D, Kim M, Vineberg KA, Balter JM. Generation of synthetic CT images from MRI for treatment planning and patient positioning using a 3-channel U-net trained on sagittal images. Front Oncol. 2019;9:964. https://doi.org/10.3389/fonc.2019.00964.
9. Qi M, Li Y, Wu A, et al. Multi-sequence MR image-based synthetic CT generation using a generative adversarial network for head and neck MRI-only radiotherapy. Med Phys. 2020;47(4):1880–94. https://doi.org/10.1002/mp.14075.
10. Wang Y, Liu C, Zhang X, Deng W. Synthetic CT generation based on T2 weighted mri of nasopharyngeal carcinoma (NPC) Using a deep convolutional neural network (DCNN). Front Oncol. 2019;9:1333. https://doi.org/10.3389/fonc.2019.01333.
11. Dinkla AM, Florkow MC, Maspero M, et al. Dosimetric evaluation of synthetic CT for head and neck radiotherapy generated by a patch-based three-dimensional convolutional neural network. Med Phys. 2019;46(9):4095–104. https://doi.org/10.1002/mp.13663.
12. Kazemifar S, McGuire S, Timmerman R, et al. MRI-only brain radiotherapy: assessing the dosimetric accuracy of synthetic CT images generated using a deep learning approach. Radiother Oncol. 2019;136:56–63. https://doi.org/10.1016/j.radonc.2019.03.026.
13. Liu F, Yadav P, Baschnagel AM, McMillan AB. MR-based treatment planning in radiation therapy using a deep learning approach. J Appl Clin Med Phys. 2019;20(3):105–14. https://doi.org/10.1002/acm2.12554.
14. Paradis E, Cao Y, Lawrence TS, et al. Assessing the dosimetric accuracy of magnetic resonance-generated synthetic CT images for focal brain VMAT radiation therapy. Int J Radiat Oncol Biol Phys. 2015;93(5):1154–61. https://doi.org/10.1016/j.ijrobp.2015.08.049.
15. Beare R, Lowekamp B, Yaniv Z. Image segmentation, registration and characterization in R with SimpleITK. J Stat Softw. 2018;86. https://doi.org/10.18637/jss.v086.i08
16. Lowekamp BC, Chen DT, Ibanez L, Blezek D. The design of SimpleITK. Front Neuroinform. 2013;7:45. https://doi.org/10.3389/fninf.2013.00045
17. Yaniv Z, Lowekamp BC, Johnson HJ, Beare R. SimpleITK image-analysis notebooks: a collaborative environment for education and reproducible research. J Digit Imaging. 2018;31(3):290–303. https://doi.org/10.1007/s10278-017-0037-8.
18. Lee S, Wolberg G, Chwa K-Y, Shin SY. Image metamorphosis with scattered feature constraints. IEEE Trans Visual Comput Graph. 1996;2(4):337–54.
19. Lee S, Wolberg G, Shin SY. Scattered data interpolation with multilevel B-splines. IEEE Trans Visual Comput Graph. 1997;3(3):228–44.
20. Mattes D, Haynor DR, Vesselle H, Lewellyn TK, Eubank W. Non-rigid multimodality image registration. Spie; 2001:1609–1620
21. Isola P, Zhu J-Y, Zhou T, Efros AA. Image-to-image translation with conditional adversarial networks. 2017:1125–1134
22. Andreasen D, Van Leemput K, Hansen RH, Andersen JA, Edmund JM. Patch-based generation of a pseudo CT from conventional MRI sequences for MRI-only radiotherapy of the brain. Med Phys. 2015;42(4):1596–605. https://doi.org/10.1118/1.4914158.
23. Gudur MS, Hara W, Le QT, Wang L, Xing L, Li R. A unifying probabilistic Bayesian approach to derive electron density from MRI for radiation therapy treatment planning. Phys Med Biol. 2014;59(21):6595–606. https://doi.org/10.1088/0031-9155/59/21/6595.
24. Hsu SH, Cao Y, Huang K, Feng M, Balter JM. Investigation of a method for generating synthetic CT models from MRI scans of the head and neck for radiation therapy. Phys Med Biol. 2013;58(23):8419–35. https://doi.org/10.1088/0031-9155/58/23/8419.
25. Huang H, Yu PS, Wang C. An introduction to image synthesis with generative adversarial nets; 2018. arXiv preprint arXiv:180304469
26. Emami H, Dong M, Nejad-Davarani SP, Glide-Hurst CK. Generating synthetic CTs from magnetic resonance images using generative adversarial networks. Med Phys. 2018; https://doi.org/10.1002/mp.13047
27. Nie D, Trullo R, Lian J, et al. Medical image synthesis with deep convolutional adversarial networks. IEEE Trans Biomed Eng. 2018;65(12):2720–30. https://doi.org/10.1109/TBME.2018.2814538.

28. Jang H, Liu F, Zhao G, Bradshaw T, McMillan AB. Technical note: deep learning based MRAC using rapid ultrashort echo time imaging. Med Phys. 2018; https://doi.org/10.1002/mp.12964
29. Lerner M, Medin J, Jamtheim Gustafsson C, Alkner S, Siversson C, Olsson LE. Clinical validation of a commercially available deep learning software for synthetic CT generation for brain. Radiat Oncol. 2021;16(1):66. https://doi.org/10.1186/s13014-021-01794-6
30. Qiao Z, Qian Z, Tang H, et al. CorGAN: Context aware recurrent generative adversarial network for medical image generation. IEEE; 2020:1100–1103